Chemical Engineering Journal 374 (2019) 91–99

Contents lists available at ScienceDirect

Chemical Engineering Journal

journal homepage: www.elsevier.com/locate/cej

Metal-organic frameworks derived magnetic carbon-αFe/Fe_3C composites as a highly effective adsorbent for tetracycline removal from aqueous solution

Weiping Xiong[a,1], Zhuotong Zeng[b,1], Guangming Zeng[a,*], Zhaohui Yang[a,*], Rong Xiao[b,*], Xin Li[a], Jiao Cao[a], Chengyun Zhou[a], Hongbo Chen[c], Meiying Jia[a], Yang Yang[a], Wenjun Wang[a], Xiang Tang[a]

[a] College of Environmental Science and Engineering, Hunan University and Key Laboratory of Environmental Biology and Pollution Control, Ministry of Education, Hunan University, Changsha 410082, China
[b] Department of Dermatology, Second Xiangya Hospital, Central South University, Changsha 410011, Hunan, China
[c] College of Environment and Resources, Xiangtan University, Xiangtan 411105, China

HIGHLIGHTS

- Magnetic carbon-αFe/Fe_3C composites were applied to remove tetracycline for the first time.
- Magnetic carbon-αFe/Fe_3C showed the higher adsorption capacity for TCN.
- Pore filling effect and electrostatic adsorption were possible adsorption mechanisms.
- Magnetic carbon-αFe/Fe_3C was suggested as a reusable and efficient adsorbent.

GRAPHICAL ABSTRACT

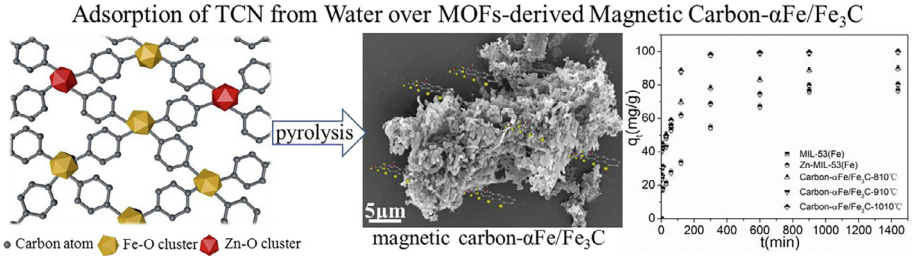

ARTICLE INFO

Keywords:
Tetracycline removal
Magnetic carbon-αFe/Fe_3C
Electrostatic adsorption
Practical application

ABSTRACT

Efficient removal of tetracycline (TCN) from aqueous solution is important for water environment security. Herein, magnetic carbon-αFe/Fe_3C derived from metal-organic frameworks (MOFs) were synthesized by a carbonization method and used for TCN adsorption. The magnetic carbon-αFe/Fe_3C adsorbent was characterized by scanning electron microscope (SEM), energy dispersive X-ray spectroscopy (EDS), X-ray diffraction (XRD), Brunauer-Emmett-Teller (BET), thermal gravimetric analyzer (TGA), X-ray photoelectron spectrum (XPS) and vibrating sample magnetometer (VSM). The resultant magnetic carbon-αFe/Fe_3C exhibited outstanding TCN adsorption capacity (511.06 mg g^{-1}) from aqueous solution due to its large specific surface area (171.72 m^2 g^{-1}) and pore volume (0.31 cm^3 g^{-1}), and abundant active adsorption sites. The main adsorption mechanisms were physisorption and chemisorption, including pore filling effect and electrostatic adsorption. Moreover, magnetic carbon-αFe/Fe_3C could remove TCN at low concentrations (< 5 mg L^{-1}) in aqueous solution to a relatively low level, which was very significant for the actual application. The high absorbability and good reusability in real water samples insured the magnetic carbon-αFe/Fe_3C with great potential in practical application.

* Corresponding authors.
E-mail addresses: zgming@hnu.edu.cn (G. Zeng), yzh@hnu.edu.cn (Z. Yang), xiaorong65@csu.edu.cn (R. Xiao).
[1] These authors contribute equally to this article.

https://doi.org/10.1016/j.cej.2019.05.164
Received 18 April 2019; Received in revised form 21 May 2019; Accepted 23 May 2019
Available online 24 May 2019
1385-8947/

1. Introduction

Antibiotics as the antibacterial agents are widely used for the treatment and prevention of diseases for human and animal, as they could effectively inhibit and kill bacteria [1,2]. However, only less than 30% of antibiotics could be adsorbed by the human or animal and most of antibiotics are discharged into water resources via urine and could cause serious water pollution [3–5]. As a typical antibiotic, the production and usage of tetracycline (TCN) was the world's second, and its concentration in wastewater from aquaculture farms reached 20 mg L^{-1} [6,7]. TCN cannot be easily biodegraded or removed by conventional wastewater treatment plant (WWTPs) because of its high stability, causing residual tetracycline to be detected in surface water and drinking water [8,9]. Residual tetracycline will accumulate in the aquatic ecosystem, which may lead to the significant increase of antibiotic resistance of microorganisms [10,11]. In the long term, TCN may eventually enter the human body through the food chain, posing significant long-term threats and potential risks to ecosystems and human health [12]. Therefore, the removal of TCN from water is very crucial and valuable.

To date, methods for the efficient removal of antibiotics mainly include adsorption, photocatalytic, Fenton-like, filtration, bio-degradation and electrochemical degradation [13–22]. In contrast, adsorption proved the advantages of its low-cost effectiveness, environmental friendliness and simple operation, which has been considered as one of the most practical techniques to remove antibiotics from water. A variety of adsorbents have been applied to TCN adsorption [23–30]. Among many candidates, metal-organic frameworks (MOFs) have received more attention because of their controllable structure, good thermal stability and high adsorption capacity to TCN (up to 303 mg g^{-1}) [3,31]. Up to now, thousands of MOFs have been developed and have wide application prospects [32,33]. Iron-based metal-organic framework MIL-53(Fe), a subclass of MIL-53(M) family, is featured with chemical versatility, abundant active sites, breathing feature and water stability [34]. Besides, the Fe^{3+} metal center with common carboxylate-type ligands can be synthesized with the characteristic of water stability [35]. Generally, MIL-53(Fe) was mainly used for advanced oxidation and adsorption [34,36–38]. For example, MIL-53(Fe) and its magnetic hybrid have been used for adsorption removal of pharmaceutical pollutant and small organic molecules [34,36]. MIL-53(Fe) powders have exhibited great potential to accelerate photocatalytic degradation of organic pollutant by activating persulfate and hydrogen peroxide [37,38]. However, the crucial issues of easy recovery, regeneration and efficient adsorption are in urgent need of solution for practical application.

Fortunately, the derivatives of MOFs prepared under thermolysis conditions have some special properties, such as magnetism, large specific surface area and pore volume, which have attracted widespread research interest [39–44]. Zhan and her co-workers have reported that porous Fe_2O_3 with preserved morphologies were synthesized by the pyrolysis of the MIL-53(Fe) and applied in catalytic selective oxidation of H_2S to sulfur [39]. Han et al. have reported that the high-performance electrocatalyst synthesized by one-step carbonization of Co-doped NH_2-MIL-53(Fe) was used for oxygen evolution reaction (OER) [40]. MnO-doped Fe_3O_4@C composite particles were prepared by a one-step thermal treatment of Mn-doped MIL-53(Fe) in Ar atmosphere and exhibited lithium-storage performance [41]. Some researchers reported that N-doped Fe/Fe_3C@C electrocatalysts were synthesized by the pyrolysis of the hexamethylenetetramine incorporated MIL-100-Fe under N_2 atmosphere and had great potential to replace Pt/C for ORR in practical use [42]. Luo et al. synthesized Fe/Fe_3C@NC by using functional carbon black combined with MIL-101(Fe) as a precursor, followed by carbonization [43]. Other research results also synthesized Fe-based catalysts by one-step Fe-MIL-88B pyrolyzation to hydrogenate conversion of carbon dioxide to valuable hydrocarbons [44]. However, the aqueous adsorption of organic pollutant onto the derivatives of MOFs has not been investigated.

Within this context, we herein expect magnetic carbon-αFe/Fe_3C derived from Zn-doped MIL-53(Fe) to be an advanced adsorbent for highly effective removal of antibiotics from aqueous solutions. Therefore, this study provided magnetic carbon-αFe/Fe_3C by the pyrolysis of Zn-doped MIL-53(Fe) at different temperature (810–1010 °C) under N_2 atmosphere. Morphologies, thermostability, magnetism and elementary composition were evaluated by characterization analysis. A series of adsorption experiments were carried out under different key parameters, such as ionic strength, humic acid, pH, adsorption kinetics and isotherms. Besides, the mechanism was studied in depth during the adsorption experiments. Finally, the reusability of magnetic carbon-αFe/Fe_3C and its application in actual water environment were discussed. It is the first time that magnetic carbon-αFe/Fe_3C has been successfully applied to remove antibiotics, especially in real samples. We hope that our work can motivate more researches on derivatives of MOFs to be applied in the removal of water environmental pollutants.

2. Experimental section

2.1. Chemicals and materials

Zinc (II) chloride ($ZnCl_2$, 99%) was received from Xiya Reagent Co., Ltd. (Shandong, China). Iron (III) chloride hexahydrate ($FeCl_3{\cdot}6H_2O$, 99%), N, N-dimethylformamide (DMF, 99.5%), 1, 4-benzenedicarboxylic acid (1, 4-BDC, 99%) were purchased from Sinopharm Chemical Reagent Co., Ltd. (Shanghai, China). Tetracycline hydrochloride (TCN) was obtained from bomei biotechnology Co., Ltd (Hefei, China). The ultra-pure water (18.25 MΩ·cm^{-1}, produced by ultra-pure water manufacturing system, Ulpure) was used throughout the whole experiments.

2.2. Synthesis and characterization of Zn-MIL-53(Fe) and magnetic carbon-αFe/Fe_3C

In a typical synthesis, Zn-MIL-53(Fe) was prepared by the previous reported method [35]. After 0.674 g of $FeCl_3{\cdot}6H_2O$ and 0.340 g of $ZnCl_2$ were dissolved in 56 mL of DMF, 0.415 g of 1, 4-BDC was added. The resulting mixture was stirred for 2 h and then transferred into a Teflon-lined bomb and heated at 170 °C for 24 h. The suspension after reaction was centrifuged. The powder product was washed with DMF and ethanol for several times, and dried at 100 °C in a vacuum. Magnetic carbon-αFe/Fe_3C was synthesized by carbonization of Zn-MIL-53(Fe) under a nitrogen atmosphere with a heating rate of 5 °C min^{-1} at different temperatures (810, 910, or 1010 °C) for 2 h. And then, the temperature cooled naturally to room temperature. These obtained black powder products were denoted as magnetic carbon-αFe/Fe_3C-810, magnetic carbon-αFe/Fe_3C-910 and magnetic carbon-αFe/Fe_3C-1010, respectively.

The surface morphology of Zn-MIL-53(Fe) and magnetic carbon-αFe/Fe_3C-910 was examined by scanning electron microscope (SEM). The energy dispersive X-ray spectroscopy (EDS) of Zn-MIL-53(Fe) and magnetic carbon-αFe/Fe_3C-910 was obtained using an energy dispersive X-ray detector. The crystal phase of MIL-53(Fe), Zn-MIL-53(Fe) and magnetic carbon-αFe/Fe_3C was analyzed by X-ray diffraction (XRD). The Brunauer-Emmett-Teller (BET) specific surface area and pore size distribution of MIL-53(Fe), Zn-MIL-53(Fe) and magnetic carbon-αFe/Fe_3C were studied by nitrogen adsorption/desorption method. The thermostability of magnetic carbon-αFe/Fe_3C was measured by thermal gravimetric analyzer (TGA). The surface composition of MIL-53(Fe), Zn-MIL-53(Fe) and magnetic carbon-αFe/Fe_3C was studied by an X-ray photoelectron spectrum (XPS). The magnetic property of magnetic carbon-αFe/Fe_3C-910 was measured by vibrating sample magnetometer (VSM).

2.3. Batch adsorption experiments

The stock TCN solution (150 mg L^{-1}) was obtained by dissolving TCN in ultrapure water, and the solutions (5–150 mg L^{-1}) with different concentrations of TCN needed in the subsequent adsorption experiments were made by diluting the stock TCN solution with ultrapure water. In order to explore the adsorption properties of materials to TCN, 10 mg of MIL-53(Fe), Zn-MIL-53(Fe), magnetic carbon-αFe/Fe_3C-810, magnetic carbon-αFe/Fe_3C-910, magnetic carbon-αFe/Fe_3C-1010 were added to 20 mg L^{-1} of TCN solution and then shaken at 25 °C with a speed of 200 rpm, respectively. Adsorption kinetic experiments were conducted with TCN concentration of 20 mg L^{-1} in solution, while the amount of adsorbents was kept at 10 mg in 50 mL of TCN solution. The mixtures were shaken under room temperature (25 °C) with a speed of 200 rpm in a gyratory shaker. For adsorption isotherm studies, 10 mg of adsorbents were added into 50 mL solutions containing 5–150 mg L^{-1} different concentrations of TCN and shaken at 25 °C, 35 °C and 45 °C with a speed of 200 rpm for 24 h, respectively. After the mixture was centrifuged at 5000 rpm for 5 min, the residual TCN concentrations in the solution were measured by a UV–vis spectrophotometer (UV-2700, Shimadzu, Japan) at 357 nm.

The effect of pH on adsorption of TCN was tested by performing adsorption experiments with the pH range of 2.0–12.0 at the TCN concentration of 20 mg L^{-1} and adsorbent dosages of 0.2 g L^{-1}. The removal of TCN by magnetic carbon-αFe/Fe_3C-910 was researched in the presence of different ionic strengths, humic acid and actual wastewater. To evaluate the reusability of magnetic carbon-αFe/Fe_3C-910, 10 mg of adsorbent was added to 50 mL solution containing 20 mg L^{-1} concentration of TCN. After shaking at 25 °C with a speed of 200 rpm, the employed adsorbent was transferred to ethyl alcohol (0.5 mol L^{-1}) and dried in a vacuum oven at 150 °C for 24 h. All the adsorption experiments were conducted in triplicates. The detailed equations and models were shown in the Table S1.

3. Results and discussion

3.1. Characterization of the adsorbents

The synthesized MIL-53(Fe) exhibited typical diffraction peaks at 9.28, 12.57, 17.68, 18.39, 25.57 and 27.36 in XRD patterns (Fig. 1), consistent with the literature [35,45]. For the Zn-MIL-53(Fe) sample, a majority of characteristic peaks are good consistent with the main characteristic peaks of MIL-53(Fe), although there were some peaks that vary in height and strength. Besides, some new diffraction peaks,

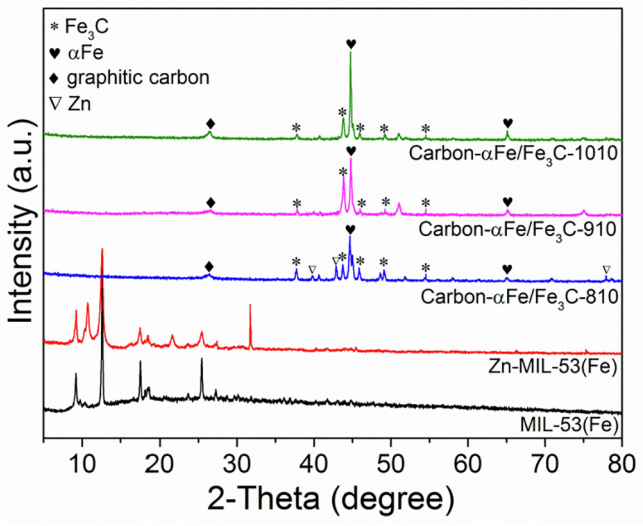

Fig. 1. The XRD spectrum of the prepared adsorbents.

typical characteristic for zinc ion, were observed. Compared with MIL-53(Fe) and Zn-MIL-53(Fe), the typical diffraction peaks of magnetic carbon-αFe/Fe_3C-810, magnetic carbon-αFe/Fe_3C-910 and magnetic carbon-αFe/Fe_3C-1010 disappeared because the high annealing temperature destroyed the crystal structure of Zn-MIL-53(Fe). The characteristic peaks at 39.16, 43.03 and 77.82 are consistent with the Zn (JCPDS card No. 04-0831) during annealing at 810 °C for 2 h for the magnetic carbon-αFe/Fe_3C-810. Additionally, the Zn peaks disappeared with the increase of annealing temperature for the magnetic carbon-αFe/Fe_3C-910 and magnetic carbon-αFe/Fe_3C-1010 because of the volatilization of zinc. After the carbonization of Zn-MIL-53(Fe), the characteristic peaks at 37.83, 43.84, 46.11, 49.18 and 54.52 of Fe_3C species (JCPDS, No. 892867), as well as the characteristic peaks at 45 and 65 of αFe (JCPDS, No. 870722), were observed in the XRD peaks of magnetic carbon-αFe/Fe_3C-810, magnetic carbon-αFe/Fe_3C-910 and magnetic carbon-αFe/Fe_3C-1010 [46]. Besides, the peak at 26.6 of graphitic carbon also can be observed, indicating that there is a special graphite structure.

The typical SEM images exhibited the morphologies of the as-synthesized Zn-MIL-53(Fe) and magnetic carbon-αFe/Fe_3C-910 was shown in Fig. 2a, c and b, d. The element (C, O, Fe and Zn) composition of Zn-MIL-53(Fe) and magnetic carbon-αFe/Fe_3C-910 was confirmed by EDS associated with SEM in Fig. 2e–n. It was observed that the Zn-MIL-53(Fe) exhibited regular spindle structures. However, the morphology of magnetic carbon-αFe/Fe_3C-910 changed a lot and became cellular structures after carbonization, demonstrating that framework structures of Zn-MIL-53(Fe) were destroyed. The results of EDS mappings indicated that zinc was successfully doped into Zn-MIL-53(Fe) but in small amounts and zinc didn't exist in this magnetic carbon-αFe/Fe_3C-910 because of the volatilization of zinc, which was in accordance with XRD analysis. From the ICP-AES analysis, the doped amount of Zn into MIL-53(Fe) was only 0.46 wt%, which confirmed the SEM result of low Zn content.

XPS was used to further explore the elemental composition and chemical states of absorbent materials. As shown in Fig. 3a, the survey spectrum indicated that zinc was successfully doped into Zn-MIL-53(Fe) and Zn peaks disappeared for the magnetic carbon-αFe/Fe_3C-910 because of the volatilization of zinc, which was also consistent with XRD and SEM analyses. The spectrum of Fe 2p (Fig. 3b) showed four main peaks at 707.65, 711.12, 720.15 and 724.39 eV, which were assigned to Fe^0 $2p_{3/2}$, Fe^{3+} $2p_{3/2}$, Fe^0 $2p_{1/2}$ and Fe^{3+} $2p_{1/2}$ respectively, demonstrating the presence of Fe and Fe_3C [42,46]. The C1s spectrum (Fig. 3c) exhibited one peak at 384.78 eV, which corresponded to C—C/C=C. The magnetic property of magnetic carbon-αFe/Fe_3C 910 was measured by VSM system at room temperature, with the field sweeping from −20,000 to +20,000 Oe in Fig. 3d. The magnetization saturation values (Ms) of magnetic carbon-αFe/Fe_3C 910 was 55.51 emu g^{-1}. The curve also showed that the magnetic carbon-αFe/Fe_3C 910 exhibited a hysteretic behavior. The magnetic performance of magnetic carbon-αFe/Fe_3C 910 was shown on the upper inset image of Fig. 3d. As displayed in the bottom inset image of Fig. 3d, this adsorption material of magnetic carbon-αFe/Fe_3C 910 was quickly attracted by the magnet. It was noteworthy that the coercivity (Hc) value for magnetic carbon-αFe/Fe_3C 910 was 181.61 Oe. In conclusion, the magnetism of magnetic carbon-αFe/Fe_3C 910 ensured that this adsorbent can be easily separated from the aqueous solution.

The N_2 adsorption-desorption isotherms of MIL-53(Fe), Zn-MIL-53(Fe), magnetic carbon-αFe/Fe_3C 810, magnetic carbon-αFe/Fe_3C 910 and magnetic carbon-αFe/Fe_3C 1010 were presented in Fig. 4. The type IV isotherms with a type H_3 hysteresis were also obviously shown in Fig. 4a, which demonstrated the existence of macroporous and mesoporous structure [47]. The pore size distributions of MIL-53(Fe), Zn-MIL-53(Fe), magnetic carbon-αFe/Fe_3C 810, magnetic carbon-αFe/Fe_3C 910 and magnetic carbon-αFe/Fe_3C 1010 were mainly concentrated in 8.812, 5.336, 7.721, 8.687 and 9.520 nm (Fig. 4b), and the BET surface areas of adsorption materials were 52.177, 46.990,

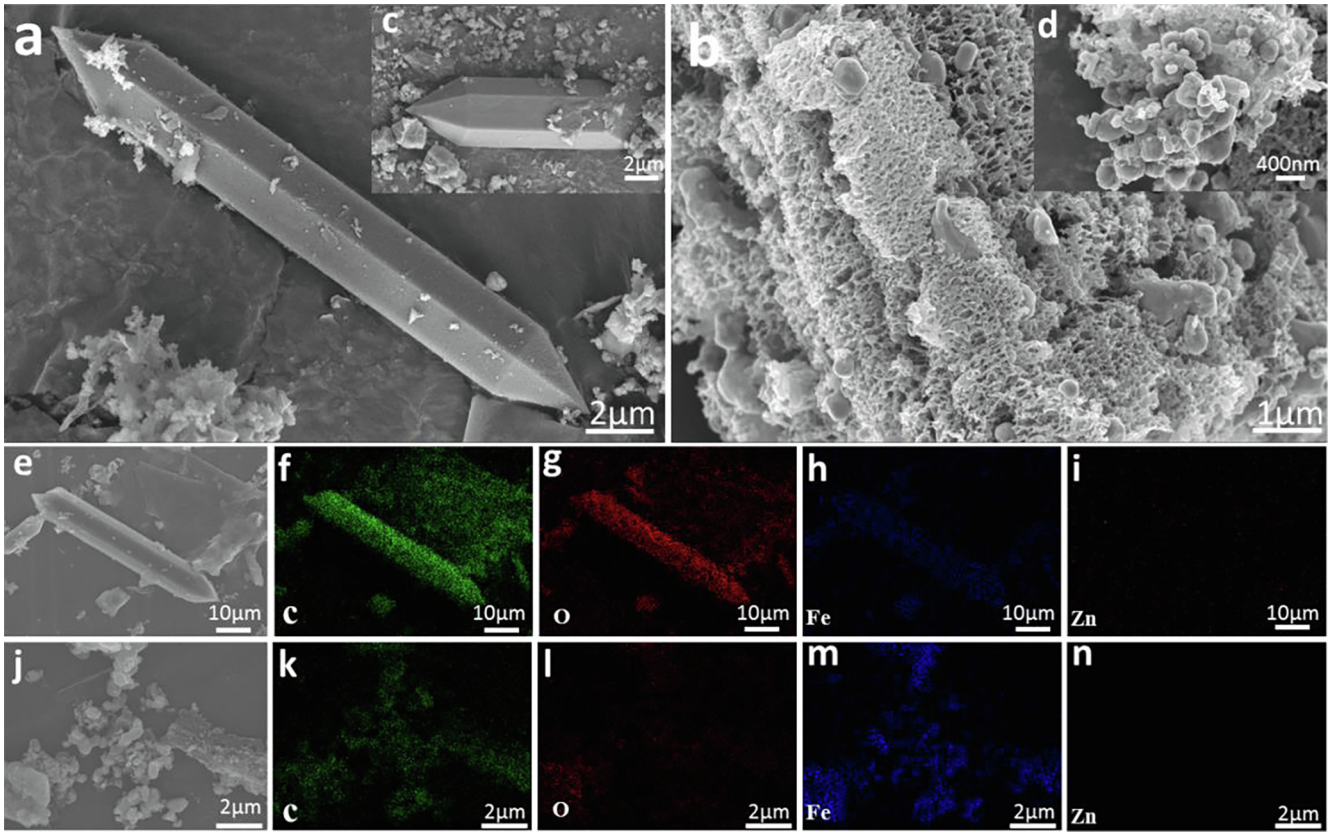

Fig. 2. The SEM images of Zn-MIL-53(Fe) (a and c) and magnetic carbon-αFe/Fe_3C-910 (b and d), SEM-EDS elemental mapping images of Zn-MIL-53(Fe) (e–i) and magnetic carbon-αFe/Fe_3C-910 (j–n).

147.293, 171.715 and 174.484 $m^2\ g^{-1}$, respectively. These adsorption materials exhibited pore volume distribution of mesoporous and macroporous, which was in accordance with the results in Table 1. The magnetic carbon-αFe/Fe_3C 1010 with relatively large specific surface area and pore volume was involved in facilitating material transfer and provided additional adsorption sites to enhance adsorption capacity. The thermal stability of the magnetic carbon-αFe/Fe_3C 810, magnetic carbon-αFe/Fe_3C 910 and magnetic carbon-αFe/Fe_3C 1010 was also researched in Fig. 5. The weight loss of the magnetic carbon-αFe/Fe_3C 810, magnetic carbon-αFe/Fe_3C 910 and magnetic carbon-αFe/Fe_3C 1010 was 8.23%, 7.03% and 3.65% respectively, owning to the volatilization of physical adsorption of water and residual organic components. It is obvious that the thermal stability of the carbon-αFe/Fe_3C is better with the increase of carbonization temperature.

3.2. Adsorption studies

MIL-53(Fe), Zn-MIL-53(Fe) and adsorbents synthesized at different carbonation temperatures (magnetic carbon-αFe/Fe_3C 810, magnetic carbon-αFe/Fe_3C 910 and magnetic carbon-αFe/Fe_3C 1010) showed different adsorption capacities for TCN in aqueous solution. In order to determine the optimal carbonization temperature, the adsorption experiment results are as follows. As seen in Fig. S1, the adsorption capacity of magnetic carbon-αFe/Fe_3C 810, magnetic carbon-αFe/Fe_3C 910 and magnetic carbon-αFe/Fe_3C 1010 was much greater than MIL-53(Fe) and Zn-MIL-53(Fe), owning to the BET surface area, pore size and total pore volume increasing significantly after the carbonization of Zn-MIL-53(Fe). Compared the magnetic carbon-αFe/Fe_3C 910 and magnetic carbon-αFe/Fe_3C 1010, the adsorption capacity of magnetic carbon-αFe/Fe_3C 1010 was slightly higher but the cost was high. Therefore, magnetic carbon-αFe/Fe_3C 910 as the optimal adsorbent was used in whole experiment.

3.2.1. Adsorption kinetics and isotherms

Adsorption kinetics of different concentrations of TCN by magnetic carbon-αFe/Fe_3C 910 was researched and the results were shown in Fig. 6a, b. It can be found by fitting the experimental data with the models that the fitting degree of pseudo-second-order model is higher, indicating that chemisorption between TCN and magnetic carbon-αFe/Fe_3C 910 controlled the adsorption rate. Besides, active sites played an important role in the adsorption capacity [48]. The calculated kinetic parameters of two models were summarized in Table 2. The determination coefficients of pseudo-second-order model ($0.9961 < R^2 < 0.9999$) were higher than that of pseudo-first-order model ($0.9145 < R^2 < 0.9753$) and the calculated $q_{e,cal}$ of pseudo-second-order equation was greater alignment with the experimental $q_{e,exp}$, which implied that the adsorption of TCN mainly depended on chemical interactions. In order to further elucidate the diffusion mechanism in the whole process of adsorption, the intra-particle diffusion model was utilized. It was obvious that the intra-particle diffusion in different concentrations of TCN presented in two distinct regions (Fig. 6c), which was mainly attributed to two factors such as external mass transfer and internal particle diffusion [49]. The first linear region was the fast adsorption process, owning to macropore diffusion on the magnetic carbon-αFe/Fe_3C 910. Besides, the second linear region was a relatively slow and gradual equilibrium adsorption process, this may be attributed to micropore diffusion [50]. As seen in Table S2, all linear portions didn't go through the origin, suggesting that intra-particle diffusion was not just a rate-limiting step [51].

Adsorption isotherms of magnetic carbon-αFe/Fe_3C 910 at different temperatures are shown in Fig. 6d, e, f. All the experimental data fitted the Langmuir, Freundlich and Temkin models well in Table 3, while the determination coefficients ($0.9957 < R^2 < 0.9987$) of Langmuir model were much higher than that of Freundlich ($0.8354 < R^2 < 0.8434$) and Temkin ($0.8802 < R^2 < 0.8825$)

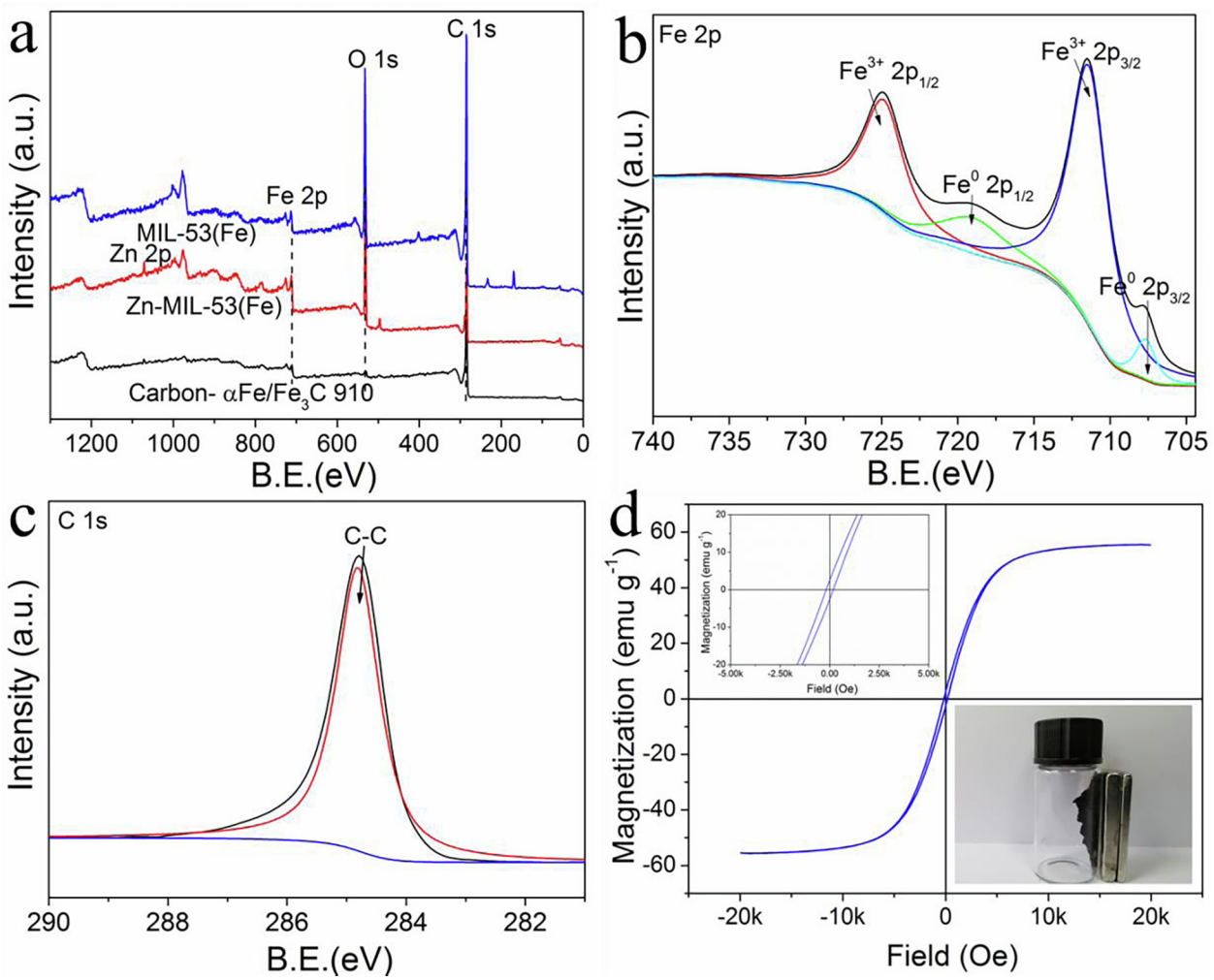

Fig. 3. The XPS spectra of the prepared adsorbents: (a) the full XPS spectra of magnetic carbon-αFe/Fe_3C-910, (b) Fe 2p, (c) C 1s; (d) room-temperature magnetization curve of magnetic carbon-αFe/Fe_3C-910.

models, which indicated that the homogeneous adsorption of TCN occurred on the magnetic carbon-αFe/Fe_3C 910. A separation factor (R_L) was used for a more in-depth study on Langmuir isotherm. As seen in Table 3, all the values of the calculated parameters (R_L) were between 0 and 1, indicating that the adsorption process of Langmuir isotherm was favorable. Moreover, the lower R_L values demonstrated that the interaction between TCN and magnetic carbon-αFe/Fe_3C 910 was comparatively strong [52]. It is well-known that absorbent materials with a large affinity coefficient (K_L) could have a large adsorption capacity (q_e) [53]. The affinity coefficient of magnetic carbon-αFe/Fe_3C 910 increased with the increase of temperature, indicating that high temperature could increase the adsorption capacity of magnetic carbon-αFe/Fe_3C 910. For further analysis of the affinity coefficient (K_L) depending on the Langmuir model at different TCN concentrations, two

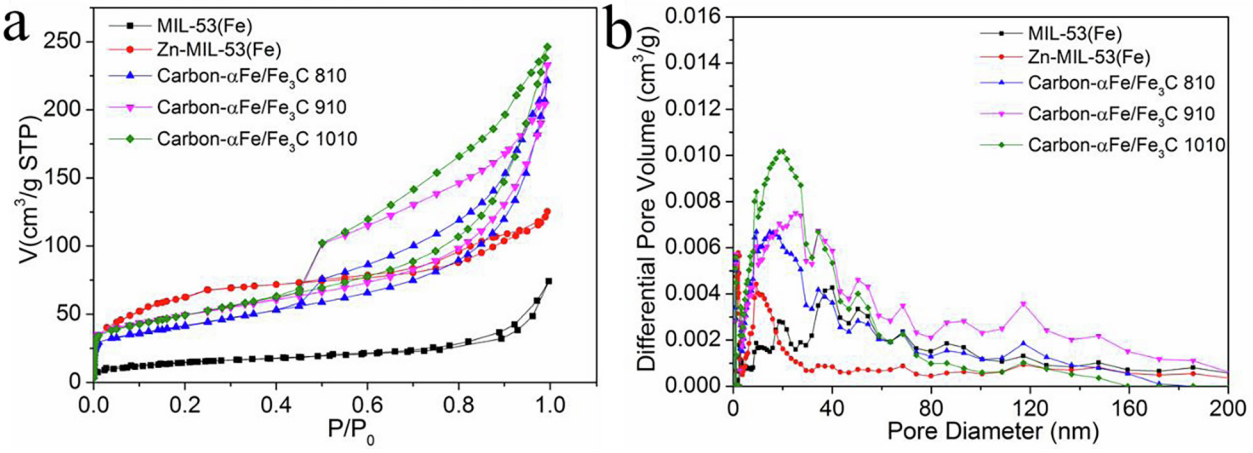

Fig. 4. N_2 adsorption-desorption isotherms (a) and pore size distribution (b) of the prepared adsorbents.

Table 1
Parameters of the porous structure for adsorbents.

Sample	S_{BET} ($m^2\ g^{-1}$)	V_t ($cm^3\ g^{-1}$)	V_{mic} ($cm^3\ g^{-1}$)	V_{mes} ($cm^3\ g^{-1}$)	V_{mac} ($cm^3\ g^{-1}$)	Pore Size (nm)
MIL-53(Fe)	52.177	0.115	0.004	0.066	0.045	8.812
Zn-MIL-53(Fe)	46.990	0.105	0.009	0.086	0.010	5.336
Carbon-αFe/Fe_3C 810	147.293	0.288	0.003	0.247	0.038	7.721
Carbon-αFe/Fe_3C 910	171.715	0.312	0.003	0.260	0.049	8.687
Carbon-αFe/Fe_3C 1010	174.484	0.349	0.003	0.314	0.032	9.520

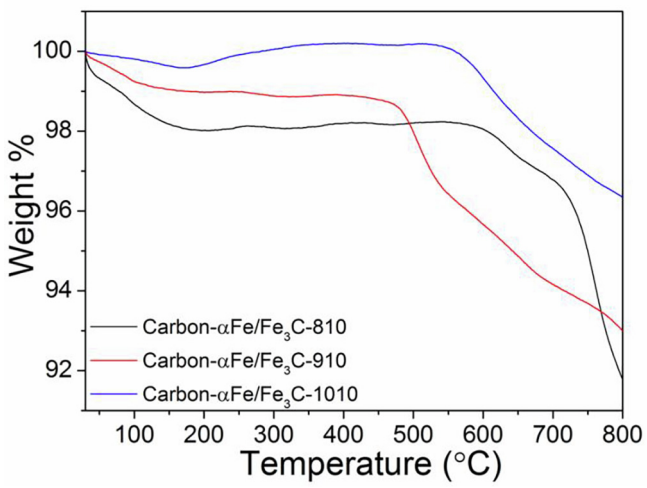

Fig. 5. Thermogravimetric analysis profiles of magnetic carbon-αFe/Fe_3C-910. Flow rate of N_2, 100 mL min^{-1}; ramping rate, 10 °C min^{-1}.

single point sorption coefficients ($K_{0.03}$, $K_{0.3}$) were calculated [54]. As shown in Table 3, the values of $K_{0.03}$ and $K_{0.3}$ increased with the increase of temperature. The higher affinity coefficients indicated the higher adsorption capacity of magnetic carbon-αFe/Fe_3C 910 at low TCN concentrations, which was very significant for the actual application of magnetic carbon-αFe/Fe_3C 910. In addition, the adsorption performance of TCN on magnetic carbon-αFe/Fe_3C 910 has been compared with other samples reported, and the results were shown in Table S3. It was easy to see that the adsorption performance of magnetic carbon-αFe/Fe_3C 910 was better than that of other adsorbents.

3.2.2. Thermodynamic analysis

The results of thermodynamics were listed in Table 4 and indicated that higher temperature as far as possible would facilitate TCN adsorption on the carbon-αFe/Fe_3C 910. All the results of ΔG were −30.548, −32.005 and −32.729 kJ mol^{-1} at 25, 35 and 45 °C, respectively, demonstrating that TCN adsorption onto magnetic carbon-αFe/Fe_3C 910 was spontaneous and thermodynamically favorable [55]. Moreover, the value of ΔH was 37.981 kJ mol^{-1}, which revealed a typical endothermic process. And this result was consistent with isothermal analysis [56]. The positive value of ΔS (0.240 kJ mol^{-1}) manifested that the randomness of the TCN adsorbed state [57,58].

3.2.3. The effect of ionic strength, humic acid and pH

The effect of ionic strength on TCN removal by magnetic carbon-αFe/Fe_3C 910 was exhibited in Fig. S2a. Sodium chloride (0.1, 0.2, 0.3, 0.4 and 0.5 mol L^{-1}) was added in TCN solutions (20 mg L^{-1}). Clearly, the adsorption capacity of TCN decreased with the addition of Sodium chloride, demonstrating that electrostatic interaction played a certain role in the adsorption process. Simultaneously, the significant decrease might be ascribed to the active sites competition on magnetic carbon-

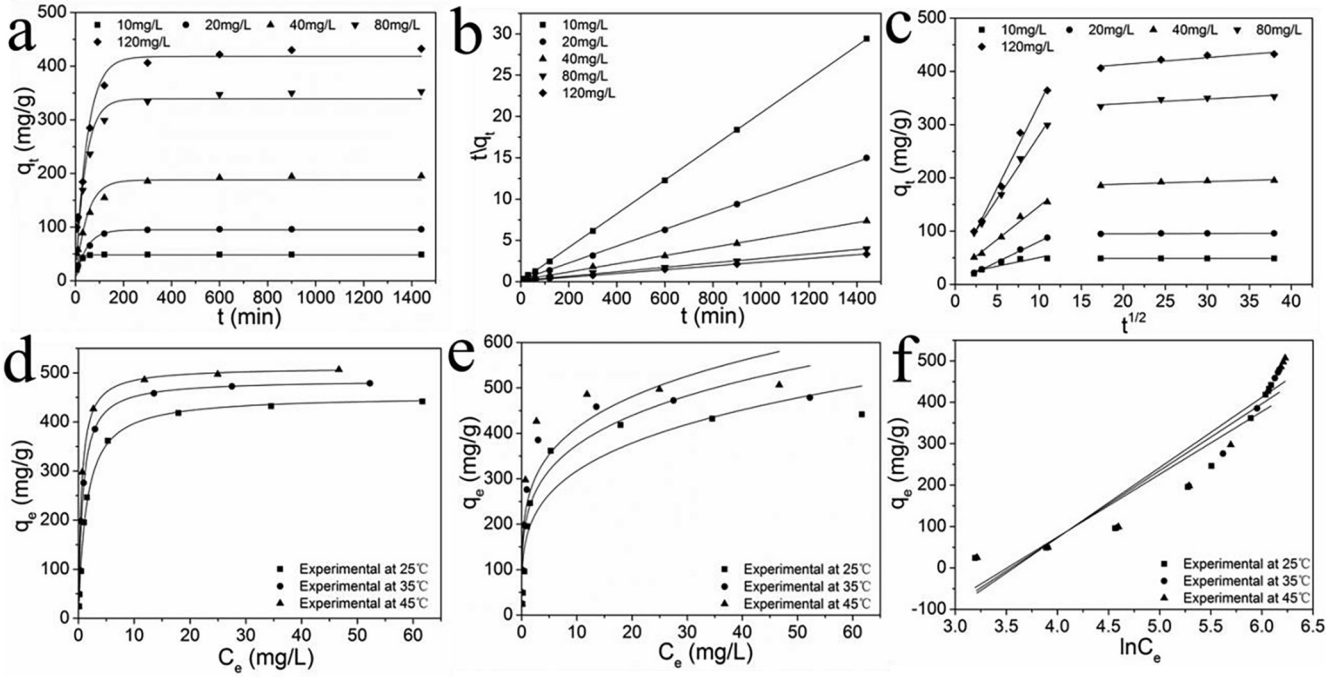

Fig. 6. The pseudo-first order plots for TCN (a) adsorption; the pseudo-second order plots for TCN (b) adsorption. The intra-particle diffusion model for TCN (c) adsorption. The Langmuir isotherm model for TCN (d) adsorption; the Frendich isotherm model for TCN (e) adsorption; the Temkin isotherm model for TCN (f) adsorption. Reaction conditions: adsorbent loading = 0.2 g L^{-1}; temperature = 25 °C; initial pH = 7.

Table 2
Adsorption kinetics parameters of TCN at different initial TCN concentration.

Concentration of TCN C_0 (mg/L)	Pseudo-first-order				Pseudo-second-order		
	q_e,exp (mg g^{-1})	q_e,cal (mg g^{-1})	k_1 (1 min^{-1})	R^2	q_e,cal (mg g^{-1})	k_2 (1 min^{-1})	R^2
10	98.95	48.37	8.96×10^{-2}	0.9753	49.16	4.53×10^{-3}	0.9999
20	98.18	95.10	2.23×10^{-2}	0.9601	98.14	4.41×10^{-4}	0.9993
40	197.42	188.01	2.15×10^{-2}	0.9180	200.80	1.32×10^{-4}	0.9985
80	382.79	339.25	2.43×10^{-2}	0.9145	371.75	5.60×10^{-5}	0.9961
120	432.31	418.05	2.08×10^{-2}	0.9532	438.60	6.23×10^{-5}	0.9988

αFe/Fe_3C 910 between TCN and sodium [58]. Humic acid containing many functional groups can interact with other materials through π-π stacking interaction, which is widely found in the actual water environment [59]. As shown in Fig. S2b, the adsorbed TCN on magnetic carbon-αFe/Fe_3C 910 decreased with high HA concentration (30 mg L^{-1}), which may be attributed to complex surface complexation in the magnetic carbon-αFe/Fe_3C 910.

The pH was considered as an important factor for the removal of TCN, owning to its impact on the presence of TCN and properties of magnetic carbon-αFe/Fe_3C 910. As shown in Fig. S3, the maximum adsorption capacity of TCN was 97.73 mg/g at pH 3, along with an appreciably decrease to 97.42 mg/g at pH 4. Whereafter, the adsorption capacity of TCN rapidly reduced with the increasing pH from 5 to 11. The adsorption trend of tetracycline was closely related to the zeta potential measurements of magnetic carbon-αFe/Fe_3C 910 in TCN solution and the dissociation constant of tetracycline, which would be discussed in depth in the mechanism analysis part.

3.3. Mechanisms for TCN adsorption

In order to further get insight into the adsorption mechanism of magnetic carbon-αFe/Fe_3C 910 toward TCN, physisorption and chemisorption were taken into account. Compared with pure MIL-53(Fe) and Zn-MIL-53(Fe) in Fig. 4 and Table 1, the specific surface area (171.715 m^2 g^{-1}) and pore volume (0.312 cm^3 g^{-1}) of magnetic carbon-αFe/Fe_3C 910 were increased to a certain extent, which provided more active adsorption sites. Correspondingly, increasing mesoporous volume (0.260 cm^3 g^{-1}) of magnetic carbon-αFe/Fe_3C 910 could weaken the steric hindrance effect and facilitate the adsorption process. Consequently, the physical adsorption was controlled by pore filling effect owning to the suitable pore size distribution.

As for the chemical adsorption, electrostatic interaction was regarded as the main chemical driving force for the removal of TCN. It was well known that the different dissociation constants (pKa) of TCN were 3.32, 7.78 and 9.58, which determined the different forms of its existence in aqueous solution, including cation (TCN^+), molecule (TCN), and anions (TCN^- and TCN^{2-}) [60]. On the other hand, the zero-potential point of magnetic carbon-αFe/Fe_3C 910 was around 2.34 in Fig. S3. The magnetic carbon-αFe/Fe_3C 910 has positive and negative surface charge at pH < 2.34 and pH > 2.34. Therefore, there was a strong repulsive force between the positive surface charge of magnetic carbon-αFe/Fe_3C 910 and the cation (TCN^+) particles at pH 2. The repulsive interaction decreased with the increased pH from 3 to 7, since TCN existed mainly in molecular form. The decrease rate of q_e increased with the increase of pH (from 8 to 11), attributing to increasing repulsive force between magnetic carbon-αFe/Fe_3C 910 and TCN. In summary, the electrostatic effect caused by the change of pH value can effectively affect TCN adsorption on magnetic carbon-αFe/Fe_3C 910. The magnetic carbon-αFe/Fe_3C 910 has a good adsorption performance in a wide pH range, which is conducive to the application in practical wastewater treatment.

Table 4
The results of thermodynamic analysis of TCN adsorption.

T (°C)	ln$K$	ΔG^θ (kJ mol^{-1})	ΔH^θ (kJ mol^{-1})	ΔS^θ (kJ mol^{-1})
25	13.459	−30.548	37.981	0.240
35	14.101	−32.005		
45	14.420	−32.729		

3.4. Adsorption behavior of magnetic carbon-αFe/Fe_3C 910 on real samples and reusability

The investigation of magnetic carbon-αFe/Fe_3C 910 adsorption properties on TCN in tap water, river water and deionized water was carried out. The quality parameters of tap water, river water and deionized water were shown in Table S4. Three kinds of tap water, river water and deionized water samples were used as the solution to provide the TCN solution (20 mg L^{-1}), respectively. The removal efficiencies of tetracycline were 95.61%, 90.27% and 99.56%, respectively, when the adsorption equilibrium was reached, which indicated that the dissolved organic matters and co-existing ions had adversely effect on the adsorption performance [61].

Table 3
Adsorption isotherm parameters of TCN at different solution temperature.

Pollutants	Isotherms	Parameters	T (°C)		
			25	35	45
TCN	Langmuir	$q_{m,cal}$(mg g^{-1})	453.51	485.66	511.06
		K_L(L mg^{-1})	0.70	1.33	1.83
		R_L	0.22	0.13	0.10
		$K_{0.03}$(L g^{-1})	310.93	621.14	886.57
		$K_{0.3}$(L g^{-1})	262.36	461.71	603.77
		R^2	0.9957	0.9979	0.9987
	Freundich	$1n^{-1}$	0.25	0.23	0.22
		K_F(L mg^{-1})	176.50	219.38	247.54
		R^2	0.8434	0.8365	0.8354
	Temkin	K_T	151.41	161.53	169.51
		f	3.00×10^{-2}	2.89×10^{-2}	2.82×10^{-2}
		R^2	0.8825	0.8802	0.8820

As shown in Fig. S4, magnetic carbon-αFe/Fe_3C 910 exhibited great reusability after five cyclic adsorption experiments. Besides, the magnetic carbon-αFe/Fe_3C 910 was easy to separate because of its magnetism and it can be readily regenerated by using ethyl alcohol on account of the solubility of TCN, which was potential in practical application in wastewater treatment.

4. Conclusion

In this work, magnetic carbon-αFe/Fe_3C with carbonization under N_2 atmosphere was prepared successfully with the obviously increased specific surface area and pore volume for highly efficient removal of TCN from aqueous solutions. The results indicated the properties of magnetic carbon-αFe/Fe_3C were significantly affected by different carbonization temperatures, and magnetic carbon-αFe/Fe_3C carbonized at 910 °C exhibited optimal adsorption capacity of TCN. It was found that the adsorption process was better fitted with pseudo-second-order and Langmuir isotherm models. Additionally, the adsorption mechanisms were dominated by electrostatic adsorption and pore filling effect. Future studies involved the effect of pH, ionic strength, humic acid and the application in actual water environment were taken into consideration. Most importantly, good reusability and magnetic separation property of magnetic carbon-αFe/Fe_3C 910 were more favorable to for potentially wider applications. We also sincerely expect that by changing functional metal ions and organic ligands with functional groups, different kinds of MOFs can yield derivatives with different superior properties for practical restoration of the water polluted with antibiotics.

Acknowledgements

The study was financially supported by the National Natural Science Foundation of China, China (81773333, 51521006, 51378190, 51578223 and 51608464), the Program for Changjiang Scholars and Innovative Research Team in University (IRT-13R17), the Natural Science Foundation of Hunan Province (2017JJ3291), the Research Foundation of Education Bureau of Hunan Province, China (17B256), the Key Research and Development Program of Hunan Province (2017SK2242).

Appendix A. Supplementary data

Supplementary data to this article can be found online at https://doi.org/10.1016/j.cej.2019.05.164.

References

[1] Y. Yang, Z.T. Zeng, C. Zhang, D.L. Huang, G.M. Zeng, R. Xiao, C. Lai, C.Y. Zhou, H. Guo, W.J. Xue, M. Cheng, W.J. Wang, J.J. Wang, Construction of iodine vacancy-rich BiOI/Ag@AgI Z-scheme heterojunction photocatalysts for visible-light-driven tetracycline degradation: transformation pathways and mechanism insight, Chem. Eng. J. 349 (2018) 808–821.
[2] H. Wang, Y. Wu, M.B. Feng, W.G. Tu, T. Xiao, T. Xiong, H.X. Ang, X.Z. Yuan, J.W. Chew, Visible-light-driven removal of tetracycline antibiotics and reclamation of hydrogen energy from natural water matrices and wastewater by polymeric carbon nitride foam, Water Res. 144 (2018) 215–225.
[3] N. Li, L. Zhou, X.Y. Jin, G. Owens, Z.L. Chen, Simultaneous removal of tetracycline and oxytetracycline antibiotics from wastewater using a ZIF-8 metal organic-framework, J. Hazard. Mater. 366 (2019) 563–572.
[4] S. Rodriguez-Mozaz, S. Chamorro, E. Marti, B. Huerta, M. Gros, A. Sànchez-Melsió, C.M. Borrego, D. Barceló, J.L. Balcázar, Occurrence of antibiotics and antibiotic resistance genes in hospital and urban wastewaters and their impact on the receiving river, Water Res. 69 (2015) 234–242.
[5] C.Y. Zhou, P. Xu, C. Lai, C. Zhang, G.M. Zeng, D.L. Huang, M. Cheng, L. Hu, W.P. Xiong, X.F. Wen, L. Qin, J.L. Yuan, W.J. Wang, Rational design of graphic carbon nitride copolymers by molecular doping for visible-light-driven degradation of aqueous sulfamethazine and hydrogen evolution, Chem. Eng. J. 359 (2019) 186–196.
[6] J.Y. Cao, L.D. Lai, B. Lai, G. Yao, X. Chen, L.P. Song, Degradation of tetracycline by peroxymonosulfate activated with zero-valent iron: performance, intermediates, toxicity and mechanism, Chem. Eng. J. 364 (2019) 45–56.
[7] T.V.R. Pillay, Aquaculture and the environment, Q. Rev. Biol. 21 (2003) 12–14.
[8] Z. Liu, J. Tian, D.B. Zeng, C.L. Yu, W.Y. Huang, K. Yang, X.Q. Liu, H. Liu, Binary-phase TiO_2 modified Bi_2MoO_6 crystal for effective removal of antibiotics under visible light illumination, Mater. Res. Bull. 112 (2019) 336–345.
[9] L.L. Ji, W. Chen, L. Duan, D.Q. Zhu, Mechanisms for strong adsorption of tetracycline to carbon nanotubes: a comparative study using activated carbon and graphite as adsorbents, Environ. Sci. Technol. 43 (2009) 2322–2327.
[10] S.J. Ye, G.M. Zeng, H.P. Wu, C. Zhang, J. Liang, J. Dai, Z.F. Liu, W.P. Xiong, J. Wan, P. Xu, M. Cheng, Co-occurrence and interactions of pollutants, and their impacts on soil remediation – a review, Crit. Rev. Environ. Sci. Technol. 47 (2017) 1528–1553.
[11] S.J. Ye, G.M. Zeng, H.P. Wu, C. Zhang, J. Dai, J. Liang, J.F. Yu, X.Y. Ren, H. Yi, M. Cheng, C. Zhang, Biological technologies for the remediation of co-contaminated soil, Crit. Rev. Biotechnol. 37 (2017) 1–15.
[12] X. Tang, G.M. Zeng, C.Z. Fan, M. Zhou, L. Tang, J.J. Zhu, J. Wan, D.L. Huang, M. Chen, P. Xu, C. Zhang, Y. Lu, W.P. Xiong, Chromosomal expression of CadR on Pseudomonas aeruginosa for the removal of Cd(II) from aqueous solutions, Sci. Total Environ. 636 (2018) 1355–1361.
[13] J.L. Gong, B. Wang, G.M. Zeng, C.P. Yang, C.G. Niu, Q.Y. Niu, W.J. Zhou, Y. Liang, Removal of cationic dyes from aqueous solution using magnetic multi-wall carbon nanotube nanocomposite as adsorbent, J. Hazard. Mater. 164 (2009) 1517–1522.
[14] Y. Yang, C. Zhang, C. Lai, G.M. Zeng, D.L. Huang, M. Cheng, J.J. Wang, F. Chen, C.Y. Zhou, W.P. Xiong, BiOX (X = Cl, Br, I) photocatalytic nanomaterials: Applications for fuels and environmental management, Adv. Colloid Interfaces 254 (2018) 76–93.
[15] Y.R. Wang, Y. Zhu, Y. Hu, G.M. Zeng, Y. Zhang, C. Zhang, C.L. Feng, How to construct DNA hydrogels for environmental applications: advanced water treatment and environmental analysis, Small 14 (2018) 1–19.
[16] C.Y. Zhou, C. Lai, C. Zhang, G.M. Zeng, D.L. Huang, M. Cheng, L. Hu, W.P. Xiong, M. Chen, J.J. Wang, Y. Yang, L.B. Jiang, Semiconductor/boron nitride composites: synthesis, properties, and photocatalysis applications, Appl. Catal. B-Environ. 238 (2018) 6–18.
[17] W.P. Xiong, J. Tong, Z.H. Yang, G.M. Zeng, Y.Y. Zhou, D.B. Wang, P.P. Song, R. Xu, C. Zhang, M. Cheng, Adsorption of phosphate from aqueous solution using iron-zirconium modified activated carbon nanofiber: performance and mechanism, J. Colloid Interf. Sci. 493 (2017) 17–23.
[18] H. Yi, M. Yan, D.L. Huang, G.M. Zeng, C. Lai, M.F. Li, X.Q. Huo, L. Qin, S.Y. Liu, X.G. Liu, B.S. Li, H. Wang, M.C. Shen, Y.K. Fu, X.Y. Guo, Synergistic effect of artificial enzyme and 2D nano-structured Bi_2WO_6 for eco-friendly and efficient biomimetic photocatalysis, Appl. Catal. B-Environ. 250 (2019) 52–62.
[19] W.J. Wang, P. Xu, M. Chen, G.M. Zeng, C. Zhang, C.Y. Zhou, Y. Yang, D.L. Huang, C. Lai, M. Cheng, L. Hu, W.P. Xiong, H. Guo, M. Zhou, Alkali metal assisted synthesis of graphite carbon nitride with tunable band-gap for enhanced visible-light-driven photocatalytic performance, ACS Sustain. Chem. Eng. 6 (2018) 15503–15516.
[20] H. Wang, Y. Sun, Y. Wu, W.G. Tu, S.Y. Wu, X.Z. Yuan, G.M. Zeng, Z.C.J. Xu, S.Z. Li, J.W. Chew, Electrical promotion of spatially photoinduced charge separation via interfacial-built-in quasi-alloying effect in hierarchical $Zn_2In_2S_5/Ti_3C_2$ (O, $OH)_x$ hybrids toward efficient photocatalytic hydrogen evolution and environmental remediation, Appl. Catal. B-Environ. 245 (2019) 290–301.
[21] H. Wang, Y. Wu, T. Xiao, X.Z. Yuan, G.M. Zeng, W.G. Tu, S.Y. Wu, H.Y. Lee, Y.Z. Tan, J.W. Chew, Formation of quasi-core-shell In_2S_3/anatase TiO_2@ metallic $Ti_3C_2T_x$ hybrids with favorable charge transfer channels for excellent visible-light-photocatalytic performance, Appl. Catal. B-Environ. 233 (2018) 213–225.
[22] L. Qin, D.L. Huang, P. Xu, G.M. Zeng, C. Lai, Y.K. Fu, H. Yi, B.S. Li, C. Zhang, M. Cheng, C.Y. Zhou, X.F. Wen, In-situ deposition of gold nanoparticles onto polydopamine-decorated g-C_3N_4 for highly efficient reduction of nitroaromatics in environmental water purification, J. Colloid Interf. Sci. 534 (2019) 357–369.
[23] P. Xu, G.M. Zeng, D.L. Huang, C.L. Feng, S. Hu, M.H. Zhao, C. Lai, Z. Wei, C. Huang, G.X. Xie, Z.F. Liu, Use of iron oxide nanomaterials in wastewater treatment: a review, Sci. Total Environ. 424 (2012) 1–10.
[24] L.H. Zhang, J.C. Zhang, G.M. Zeng, H.R. Dong, Y.N. Chen, C. Huang, Y. Zhu, R. Xu, Y.J. Cheng, K.J. Hou, W.C. Cao, W. Fang, Multivariate relationships between microbial communities and environmental variables during co-composting of sewage sludge and agricultural waste in the presence of PVP-AgNPs, Bioresour. Technol. 261 (2018) 10–18.
[25] H. Kai, G.Q. Chen, G.M. Zeng, A.W. Chen, Z.Z. Huang, J.B. Shi, T.T. Huang, M. Peng, L. Hu, Three-dimensional graphene supported catalysts for organic dyes degradation, Appl. Catal. B-Environ. 228 (2018) 19–28.
[26] K. He, Z.T. Zeng, A.W. Chen, G.M. Zeng, R. Xiao, P. Xu, Z.Z. Huang, J.B. Shi, L. Hu, G.Q. Chen, Advancement of Ag-graphene based nanocomposites: an overview of synthesis and its applications, Small 14 (2018) 1–13.
[27] Q. Lei, G.M. Zeng, C. Lai, D.L. Huang, P. Xu, C. Zhang, M. Cheng, X.G. Liu, S.Y. Liu, B.S. Li, H. Yi, "Gold rush" in modern science: fabrication strategies and typical advanced applications of gold nanoparticles in sensing, Coordin. Chem. Rev. 359 (2018) 1–31.
[28] H. Wang, Z.T. Zeng, P. Xu, L.S. Li, G.M. Zeng, R. Xiao, Z.Y. Tang, D.L. Huang, L. Tang, C. Lai, D.N. Jiang, Y. Liu, H. Yi, L. Qin, S.J. Ye, X.Y. Ren, W.W. Tang, Recent progress in covalent organic framework thin films: fabrications, applications and perspectives, Chem. Soc. Rev. 48 (2019) 488–516.
[29] S.J. Ye, M. Yan, X.F. Tan, J. Liang, G.M. Zeng, H.P. Wu, B. Song, C.Y. Zhou, Y. Yang, H. Wang, Facile assembled biochar-based nanocomposite with improved graphitization for efficient photocatalytic activity driven by visible light, Appl. Catal. B-Environ. 250 (2019) 78–88.
[30] B. Song, M. Chen, S.J. Ye, P. Xu, G.M. Zeng, J.L. Gong, J. Li, P. Zhang, W.C. Cao, Effects of multi-walled carbon nanotubes on metabolic function of the microbial community in riverine sediment contaminated with phenanthrene, Carbon 144

(2019) 1–7.
[31] D.N. Jiang, M. Chen, H. Wang, G.M. Zeng, D.L. Huang, M. Cheng, Y. Liu, W.J. Xue, Z.W. Wang, The application of different typological and structural MOFs-based materials for the dyes adsorption, Coordin. Chem. Rev. 380 (2019) 471–483.
[32] F. Hiroyasu, K.E. Cordova, O.K. Michael, O.M. Yaghi, The chemistry and applications of metal-organic frameworks, Science 341 (2013) 974–986.
[33] Q. Xia, H. Wang, B.B. Huang, X.Z. Yuan, J.J. Zhang, J. Zhang, L.B. Jiang, T. Xiong, G.M. Zeng, State-of-the-art advances and challenges of iron-based metal organic frameworks from attractive features, synthesis to multifunctional applications, Small. 15 (2019) 1803088.
[34] S. Naeimi, H. Faghihian, Application of novel metal organic framework, MIL-53(Fe) and its magnetic hybrid: for removal of pharmaceutical pollutant, doxycycline from aqueous solutions, Environ. Toxicol. Phar. 53 (2017) 121–132.
[35] W.P. Xiong, G.M. Zeng, Z.H. Yang, Y.Y. Zhou, C. Zhang, M. Cheng, Y. Liu, L. Hu, J. Wan, C.Y. Zhou, R. Xu, X. Li, Adsorption of tetracycline antibiotics from aqueous solutions on nanocomposite multi-walled carbon nanotube functionalized MIL-53(Fe) as new adsorbent, Sci. Total Environ. 627 (2018) 235–244.
[36] S. Ling, R.I. Walton, B. Slater, Theoretical study of conformational disorder and selective adsorption of small organic molecules in the flexible metal-organic framework material MIL-53-Fe, Mol. Simulat. 41 (2015) 1348–1356.
[37] L.H. Ai, C.H. Zhang, L.L. Li, J. Jing, Iron terephthalate metal-organic framework: Revealing the effective activation of hydrogen peroxide for the degradation of organic dye under visible light irradiation, Appl. Catal. B-Environ. 148 (2014) 191–200.
[38] Y.W. Gao, S.M. Li, Y.X. Li, L.Y. Yao, H. Zhang, Accelerated photocatalytic degradation of organic pollutant over metal-organic framework MIL-53(Fe) under visible LED light mediated by persulfate, Appl. Catal. B-Environ. 202 (2017) 165–174.
[39] Y.Y. Zhan, L.J. Shen, C.B. Xu, W.T. Zhao, L.L. Jiang, MOF-derived porous Fe_2O_3 with controllable shapes and improved catalytic activities in H_2S selective oxidation, CrystEngComm 20 (2018) 3449–3454.
[40] Y.J. Han, J.F. Zhai, L.L. Zhang, S.J. Dong, Direct carbonization of cobalt-doped NH_2-MIL-53(Fe) for electrocatalysis of oxygen evolution reaction, Nanoscale 8 (2015) 1033–1039.
[41] Z.S. He, K. Wang, S.S. Zhu, L.A. Huang, M.M. Chen, J.F. Guo, S.E. Pei, H.B. Shao, J.M. Wang, MOF-derived hierarchical MnO-doped Fe_3O_4@C composite nanospheres with enhanced lithium storage, ACS Appl. Mater. Inter. 10 (2018) 10974–10985.
[42] D.K. Guo, S.C. Han, J.C. Wang, Y.F. Zhu, MIL-100-Fe derived N-doped Fe/Fe_3C@C electrocatalysts for efficient oxygen reduction reaction, Appl. Surf. Sci. 434 (2018) 1266–1273.
[43] Y. Luo, J. Zhang, M. Kiani, Y.H. Chen, G. Wang, S.H. Chan, R.L. Wang, Synthesis of MOF-derived non-precious catalyst with the high electrocatalytic activity for Oxygen Reduction Reaction, Ind. Eng. Chem. Res. 57 (2018) 12087–12095.
[44] J.H. Liu, A.F. Zhang, M. Liu, S. Hu, F.S. Ding, C.S. Song, X.W. Guo, Fe-MOF-derived highly active catalysts for carbon dioxide hydrogenation to valuable hydrocarbons, J. CO2 Util. 21 (2017) 100–107.
[45] L.H. Ai, L.L. Li, C.H. Zhang, J. Fu, J. Jiang, MIL-53(Fe): a metal-organic framework with intrinsic peroxidase-like catalytic activity for colorimetric biosensing, Chemistry 19 (2013) 15105–15108.
[46] C.S. Song, S.K. Wu, X.P. Shen, X.L. Miao, Z.Y. Ji, A.H. Yuan, K.Q. Xu, M.M. Liu, X.L. Xie, L.R. Kong, G.X. Zhu, S.A. Shah, Metal-organic framework derived Fe/Fe_3C@N-doped-carbon porous hierarchical polyhedrons as bifunctional electrocatalysts for hydrogen evolution and oxygen-reduction reactions, J. Colloid Interf. Sci. 524 (2018) 93–101.
[47] H.Q. Song, Q. Zhu, X.J. Zheng, X.G. Chen, One-step synthesis of three-dimensional graphene/multiwalled carbon nanotubes/Pd composite hydrogel: an efficient recyclable catalyst for Suzuki coupling reactions, J. Mater. Chem. A 3 (2015) 10368–10377.
[48] C. Tian, J. Zhao, X.W. Ou, J.T. Wan, Y.P. Cai, Z. Lin, Z. Dang, B.S. Xing, Enhanced adsorption of p-arsanilic acid from water by amine-modified UiO-67 as examined using extended X-ray absorption fine structure, X-ray photoelectron spectroscopy, and density functional theory calculations, Environ. Sci. Technol. 52 (2018) 3466–3475.
[49] Q.Q. Song, F. Yi, Z.Y. Liu, L.L. Li, Y.R. Wang, J.L. Liang, Y. Huang, J. Lin, L. Hu, J. Zhang, C.C. Tang, The performance of porous hexagonal bn in high adsorption capacity towards antibiotics pollutants from aqueous solution, Chem. Eng. J. 325 (2017) 71–79.
[50] F.C. Wu, R.L. Tseng, R.S. Juang, Comparisons of porous and adsorption properties of carbons activated by steam and KOH, J. Colloid Interf. Sci. 283 (2005) 49–56.
[51] W.P. Xiong, Z.T. Zeng, X. Li, G.M. Zeng, R. Xiao, Z.H. Yang, Y.Y. Zhou, C. Zhang, M. Cheng, L. Hu, C.Y. Zhou, L. Qin, R. Xu, Y.R. Zhang, Multi-walled carbon nanotube/amino-functionalized MIL-53(Fe) composites: remarkable adsorptive removal of antibiotics from aqueous solutions, Chemosphere 210 (2018) 1061–1069.
[52] E.S. Ibrahim, E. Laszlo, K. Jong-Ho, S. Ho Kyong, Adsorption and photocatalytic degradation of methylene blue over hydrogen-titanate nanofibres produced by a peroxide method, Water Res. 47 (2013) 4115–4125.
[53] Q. Cao, F. Huang, Z.Y. Zhuang, Z. Lin, A study of the potential application of nano-$Mg(OH)_2$ in adsorbing low concentrations of uranyl tricarbonate from water, Nanoscale 4 (2012) 2423–2430.
[54] Z.Y. Wang, J. Zhao, L. Song, H. Mashayekhi, B. Chefetz, B.S. Xing, Adsorption and desorption of phenanthrene on carbon nanotubes in simulated gastrointestinal fluids, Environ. Sci. Technol. 45 (2011) 6018–6024.
[55] J. Cao, Z.H. Yang, W.P. Xiong, Y.Y. Zhou, Y.R. Peng, X. Li, C.Y. Zhou, R. Xu, Y.R. Zhang, One-step synthesis of Co-doped UiO-66 nanoparticle with enhanced removal efficiency of tetracycline: simultaneous adsorption and photocatalysis, Chem. Eng. J. 353 (2018) 126–137.
[56] R. Ocampo-Pérez, J. Rivera-Utrilla, C. Gómez-Pacheco, M. Sánchez-Polo, J.J. López-Peñalver, Kinetic study of tetracycline adsorption on sludge-derived adsorbents in aqueous phase, Chem. Eng. J. 213 (2012) 88–96.
[57] Y.X. Yang, X.J. Hu, Y.L. Zhao, L.H. Cui, Z.J. Huang, J.J. Long, J.W. Xu, J.B. Deng, C.Y. Wu, W.W. Liao, Decontamination of tetracycline by thiourea-dioxide-reduced magnetic graphene oxide: Effects of pH, ionic strength, and humic acid concentration, J. Colloid Interf. Sci. 495 (2017) 68–77.
[58] L. Tang, J.F. Yu, Y. Pang, G.M. Zeng, Y.C. Deng, J.J. Wang, X.Y. Ren, S.J. Ye, B. Peng, H.P. Feng, Sustainable efficient adsorbent: alkali-acid modified magnetic biochar derived from sewage sludge for aqueous organic contaminant removal, Chem. Eng. J. 336 (2018) 160–169.
[59] J.H. Jin, Z.H. Yang, W.P. Xiong, Y.Y. Zhou, R. Xu, Y.R. Zhang, J. Cao, X. Li, C.Y. Zhou, Cu and Co nanoparticles co-doped MIL-101 as a novel adsorbent for efficient removal of tetracycline from aqueous solutions, Sci. Total Environ. 650 (2019) 408–418.
[60] Z. Qiang, C. Adams, Potentiometric determination of acid dissociation constants (p) for human and veterinary antibiotics, Water Res. 38 (2004) 2874–2890.
[61] F. Chen, Q. Yang, Y. Zhong, H.X. An, J.W. Zhao, T. Xie, Q.X. Xu, X.M. Li, D.B. Wang, G.M. Zeng, Photo-reduction of bromate in drinking water by metallic Ag and reduced graphene oxide (RGO) jointly modified $BiVO_4$ under visible light irradiation, Water Res. 101 (2016) 555–563.